JACS
JOURNAL OF THE AMERICAN CHEMICAL SOCIETY
Article
pubs.acs.org/JACS

Interactions of Bacterial Cell Division Protein FtsZ with C8-Substituted Guanine Nucleotide Inhibitors. A Combined NMR, Biochemical and Molecular Modeling Perspective

Filipa Marcelo,[†,‡,#] Sonia Huecas,[†,#] Laura B. Ruiz-Ávila,[†] F. Javier Cañada,[†] Almudena Perona,[∥] Ana Poveda,[§] Sonsoles Martín-Santamaría,[⊥] Antonio Morreale,[∥,▽] Jesús Jiménez-Barbero,*[,†] and José M. Andreu*[,†]

[†]Centro de Investigaciones Biológicas, CIB-CSIC, Ramiro de Maeztu 9, 28040 Madrid, Spain
[‡]REQUIMTE, CQFB, Departamento de Química, Faculdade de Ciências e Tecnologia, UNL, 2829-516 Caparica, Portugal.
[§]Servicio Interdepartamental de Investigación, Universidad Autónoma de Madrid, Cantoblanco, 28049 Madrid, Spain
[∥]Unidad de Bioinformática, Centro de Biología Molecular, CBMSO−CSIC, Campus UAM, Madrid, Spain
[⊥]Departamento de Química, Universidad CEU-San Pablo, Madrid, Spain

Supporting Information

ABSTRACT: FtsZ is the key protein of bacterial cell-division and target for new antibiotics. Selective inhibition of FtsZ polymerization without impairing the assembly of the eukaryotic homologue tubulin was demonstrated with C8-substituted guanine nucleotides. By combining NMR techniques with biochemical and molecular modeling procedures, we have investigated the molecular recognition of C8-substituted-nucleotides by FtsZ from *Methanococcus jannaschii* (Mj-FtsZ) and *Bacillus subtilis* (Bs-FtsZ). STD epitope mapping and trNOESY bioactive conformation analysis of each nucleotide were employed to deduce differences in their recognition mode by each FtsZ species. GMP binds in the same anti conformation as GTP, whereas 8-pyrrolidino-GMP binds in the syn conformation. However, the anti conformation of 8-morpholino-GMP is selected by Bs-FtsZ, while Mj-FtsZ binds both anti- and syn-geometries. The inhibitory potencies of the C8-modified-nucleotides on the assembly of Bs-FtsZ, but not of Mj-FtsZ, correlate with their binding affinities. Thus, MorphGTP behaves as a nonhydrolyzable analog whose binding induces formation of Mj-FtsZ curved filaments, resembling polymers formed by the inactive forms of this protein. NMR data, combined with molecular modeling protocols, permit explanation of the mechanism of FtsZ assembly impairment by C8-substituted GTP analogs. The presence of the C8-substituent induces electrostatic remodeling and small structural displacements at the association interface between FtsZ monomers to form filaments, leading to complete assembly inhibition or to formation of abnormal FtsZ polymers. The inhibition of bacterial Bs-FtsZ assembly may be simply explained by steric clashes of the C8-GTP-analogs with the incoming FtsZ monomer. This information may facilitate the design of antibacterial FtsZ inhibitors replacing GTP.

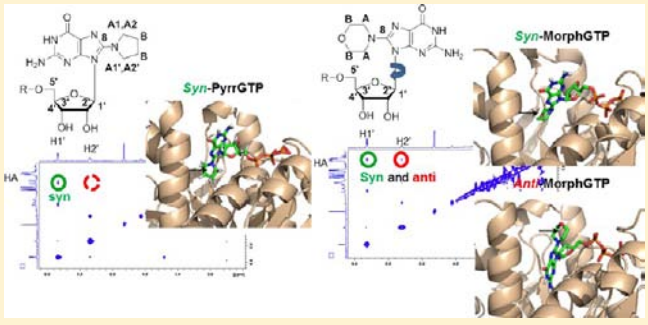

INTRODUCTION

FtsZ is the main protein that most bacteria use to divide. It has been recognized as an attractive target for new antibiotics.[1] There is a pressing need of newly identified antibacterial targets and lead compounds to develop new antibiotics that are continuously required to fight the increasing prevalence of pathogen strains resistant to current antibiotics, whose infections are a leading cause of death.[2] FtsZ forms the bacterial division ring (Z-ring), acting as a scaffold that recruits the other proteins of the division machinery.[3] FtsZ is a self-assembling cytoskeletal GTPase that shares the structural fold of eukaryotic tubulin.[4] FtsZ monomers form tubulin-like filaments in which the GTP binding site of one monomer is completed by the GTPase-activating domain of the next monomer along the filament.[5] FtsZ filaments are dynamic, bend and depolymerize upon GTP hydrolysis, and also associate among them in different fashions.[6] An array of short FtsZ filaments have been visualized by electron cryotomography,[7] whereas super resolution light microscopy has shown a discontinuous Z-ring,[8] which possibly contracts by a combination of association, recycling, sliding, and bending of FtsZ filaments. A growing number of small molecules are reported to interact with FtsZ and bacterial cell-division.[1,9] Among them, the difluorobenzamide derivative PC190723 protected mice from a lethal dose of *Staphylococcus aureus* (Sa-FtsZ) and has

Received: June 3, 2013
Published: September 30, 2013

   dx.doi.org/10.1021/ja405515r | J. Am. Chem. Soc. 2013, 135, 16418−16428

served to validate FtsZ as an effective antibacterial target.[10] This ligand binds at a narrow cleft between the N- and C-terminal domains of FtsZ,[11] probably targeting the FtsZ assembly switch, and induces the formation of FtsZ filaments and condensates,[12] impairing the correct assembly of the Z-ring.[10,13] Regarding FtsZ's nucleotide site, the natural bisdiarylbutene macrocycle crysophaentin A binds to FtsZ competitively with GTPγS in saturation transfer difference (STD) NMR experiments inhibiting FtsZ assembly and the growth of *S. aureus*.[14]

In classical GTPase switches, GTP/GDP binding induces an activating structural change in the unassociated protein.[15] In contrast, the structural switch of FtsZ assembly is thought to be induced by polymer contacts, so that GTP hydrolysis fine-tunes the switch by increasing the unfavorable free energy difference between the inactive and active FtsZ conformation.[11,16] Successful inhibitors of bacterial FtsZ must avoid poisoning tubulin, the most structurally similar mammalian protein. The modified nucleotide 8-bromoguanosine-5′-triphosphate (BrGTP), which promotes tubulin assembly, was found to inhibit polymerization and GTPase activity of FtsZ.[17] This result lead to studies probing FtsZ and tubulin with a series of C8-substituted GTP analogs.[18] It was found that GTP analogs with small substituents at C8 inhibit FtsZ polymerization and GTPase, whereas they promote normal microtubule assembly similarly to GTP. The inhibitory potencies of the C8-GTP analogs on FtsZ polymerization correlated with the available binding affinity values to the GTP site of FtsZ monomers. The 1.4 Å resolution crystal structure of a complex of FtsZ with C8-morpholino-GTP (MorphGTP) revealed nucleotide and protein conformations closely similar to the FtsZ-GDP complex.[18] This provided a proof of concept that it is possible to selectively inhibit FtsZ assembly with modified nucleotides, which can be exploited to specifically target the bacterial Z-ring.[9a] However, the FtsZ-bound conformations of the C8-nucleotide derivatives have not been determined. The steric hindrance of large substituents at C8 with the ribose moiety could favor a syn-type glycosidic torsion angle, as opposed to the natural GTP anti conformation. Therefore, the lower binding affinity observed for the more bulky C8-GTP analogs might be explained if selective binding of their anticonformation (as GTP) to FtsZ monomers would have to shift from a syn-dominated conformational equilibrium of the ligands in solution.[18] Calculated relative binding affinities to FtsZ of several C8-GTP analogs followed this trend,[19] but the hypothesis remained to be experimentally tested. In addition, the mechanism by which C8-substituted-GTP analogs inhibit FtsZ assembly was basically unknown. The binding pose of MorphGTP[18] did not predict steric clashes with the next FtsZ monomer in a growing protofilament, according to the protofilament-like structures that were then available.[5,20] It was speculated that minor shifts in protein conformation or rearrangement of water molecules at the polymerization interface could lead to the inhibition of FtsZ filament formation. The possibility that the FtsZ protofilament models available were not providing an accurate description of the true polymerization interface was also considered.[18] There was also the initially attractive possibility that the mechanism of inhibition of FtsZ assembly by the C8-GTP analogs could be related to their syn-anti conformational changes.

In this context, we have determined the free and FtsZ-bound conformations and the binding epitopes of C8-substituted guanine nucleotides with NMR experiments and two different FtsZ proteins. We have further analyzed the binding of C8-guanine nucleotides to FtsZ monomers and their inhibition of FtsZ assembly with biochemical methods. Finally, we have combined the NMR and biochemical results with molecular modeling protocols, and employed the recently available structure of a FtsZ filament,[11] to present an integrated explanation of the inhibition of FtsZ assembly by C8-GTP analogs. These modified nucleotides may serve as model inhibitors for the design of new antibacterial molecules targeting the GTP binding site of FtsZ.

EXPERIMENTAL SECTION

Nucleotides. 8-Morpholino-GTP (MorphGTP), MorphGMP, and 8-pyrrolidino-GMP (PyrrGMP) were custom synthesized by Jena Biosciences (>95% pure in HPLC) as described.[18] MeOGTP and PyrrGTP were prepared as reported[18] (provided by Dr. Tanneke den Blaauwen). Mant-GTP and Br-GTP were from Jena Biosciences. GTP, GDP, and GMP were from Sigma. [8-^{3}H]GTP (35.5 Ci/mmol) was from Perkin-Elmer. The nucleotides employed in NMR experiments were dissolved in 99.9% D_2O (Cambridge Isotope Laboratories) to a final concentration of 50 mM, neutralized with KOD when necessary, and stored at −20 °C.

Proteins Expression and Purification. Mj-FtsZ was overproduced in *E. coli* BL21(DE3) pLys, and purified as described.[21] Nucleotide-free Mj-FtsZ (apo-FtsZ) was prepared as described before.[22] Bs-FtsZ was overproduced in *E. coli* C41(DE3) cells and purified as described,[12] with minor modifications (see Supporting Information, SI, page S3).

Competition Binding Measurements with mant-GTP. Ligand competition with mant-GTP for binding to Mj-FtsZ was performed in 25 mM Pipes-KOH, 50 mM KCl, 1 mM EDTA, 10 mM $MgCl_2$, pH 7.4, employing fluorescence anisotropy.[23] To set up this procedure with Bs-FtsZ, the equilibrium binding constant of the reference ligand mant-GTP to the nucleotide binding site of Bs-FtsZ and the number of binding sites in this protein were measured first. Ligand competition with mant-GTP and Bs-FtsZ was then measured as described[23] with some modifications (see details in the SI S3).

Mj-FtsZ Polymerization and Electron Microscopy. The assembly inhibitory capacity of the GTP analogs was determined by sedimentation FtsZ polymers and electrophoresis of pellet and supernatant (see SI S4). Noncentrifuged samples (10−20 μL) were adsorbed to carbon-coated copper electron microscopy grids and negatively stained with 2% uranyl acetate. Micrographs were taken at ×30 000 magnification in a Jeol 1230 electron microscope operated at 100 kV.

Preparations of Proteins for NMR-STD and trNOESY Experiments. Before performing the NMR experiments, apo-FtsZ and Bs-FtsZ were equilibrated in 25 mM Tris-DCl buffer, 50 mM KCl, 1 mM EDTA in 99.9% D_2O, uncorrected pH meter reading 7.4 (D_2O buffer), in a Fast Desalting Column HR 10/10 (Pharmacia Biotech) and then concentrated with a D_2O prewashed Centricon YM10 (Millipore) filter in the cold. The concentration of apo-FtsZ was measured spectrophotometrically employing an extinction coefficient of ε280 nm = 6990 M^{-1} cm^{-1}.[22] The concentration of Bs-FtsZ was measured in GdmCl[12] or employing practical extinction coefficient values determined for the purified protein preparations in buffer (ε280 nm ≈ 2980 M^{-1} cm^{-1}). $MgCl_2$ was added to a final concentration of 10 mM from a 1 M solution in D_2O, except when indicated.

Analytical Ultracentrifugation and Association State. We analyzed the association state of both proteins under our NMR experimental conditions (D_2O buffer), employing sedimentation velocity measurements (Figure S2 in SI S5) that were made in a Beckman Optima XL-I analytical ultracentrifuge (AUC) with interference optics, using an An50/Ti rotor with 12-mm double-sector centerpieces at 50 000 rpm and 25 °C. Differential sedimentation coefficient distributions, c(s), were calculated with SEDFIT.[24] The weight average sedimentation coefficient values measured in D_2O buffer at 25 °C were corrected to H_2O at 20 °C ($s_{20,w}$).

The sedimentation coefficient distributions of Mj-FtsZ (30 μM) with GMP and C8-GMP derivatives (1.2 mM) were very similar, showing a fraction (7−16%) of $s_{20,w}$ = 3.6 S FtsZ monomers,[25] a majority (77−83%) of a 6.2 S sedimentation boundary compatible with FtsZ dimer and trimer formation, fewer (8−9%) 8.6 S and (2−4%) 11.0 S oligomers, as calculated with SEDFIT. Very similar results were obtained with GTP without $MgCl_2$. These results indicate that the group present in the C8 position does not interfere with the known nonspecific Mj-FtsZ oligomerization,[21] which should not interfere with NMR ligand epitope mapping and conformational analysis. The sedimentation coefficient distributions for Bs-FtsZ in the presence of GMP or MeOGMP (1.2 mM) showed one major fraction (95−98%) of an $s_{20,w}$ = 3.5 S sedimentation boundary compatible with FtsZ monomers, but with PyrrGMP or MorphGMP (1.2 mM) showed two equally distributed fractions (43−53%) of 3.4 S monomers and (46−58%) 4.7 S dimers. The data indicate that these bulky groups induce a partial Bs-FtsZ dimerization at relatively high protein concentrations, which does not progress into formation of polymers that would sediment to the bottom of the AUC cell. The STD and trNOESY results with Bs-FtsZ could be explained by binding to the monomer nucleotide site, irrespective of the dimers induced by MorphGMP and PyrrGMP. Nevertheless, these dimers should have distorted association interfaces, in order to explain the observed inhibition of Bs-FtsZ assembly by the corresponding nucleotide triphosphates (see Discussion).

NMR Experiments. All NMR experiments were recorded on a Bruker 600 MHz spectrometer equipped with a triple channel cryoprobe head. For the experiments of the free ligands, a solution of the corresponding nucleotide was prepared in D_2O buffer. For the binding studies, Mj-FtsZ and Bs-FtsZ were equilibrated in D_2O buffer as described above. D_2O was employed as solvent to facilitate the water suppression protocol and good monitoring of the nonexchangeable protons of the ligands, which bear most of the key conformational (and epitope) information. STD-NMR experiments were performed for 40:1 and 80:1 nucleotide/protein molar ratios at 298 K, using a protein concentration of 30 μM. 1D and 2D trNOESY data were recorded using mixing times of 100 and 200 ms at 298 K, with 10:1 and 20:1 nucleotide/protein molar ratios. ^{31}P experiments were performed at 202.404 MHz (for ^{31}P), using a QNP ^{1}H-^{13}C/^{15}N/^{31}P probe. Further details are described in SI S6.

Docking and Molecular Dynamics Simulations (MD). The structures of Mj-FtsZ monomers complexed with GTP-Mg^{2+} or GDP were taken from the PDB entries 1w5a and 2vap, respectively. The structure of Bs-FtsZ was PDB 2vxy. Initial docking solutions of the C8-nucleotides into the FtsZ binding site were selected accordingly to the STD epitope mapping and the trNOESY results. The complexes were then subjected to 10 ns MD simulations performed with the AMBER 11 package.[26] A Bs-FtsZ dimer was first built by superimposing 2vxy monomers onto 1w5a subunits. A second Bs-FtsZ dimer was modeled onto the filament structure of Sa-FtsZ (PDB 3vo8). For further computational details, see SI S7, S8, and S28.

RESULTS

Conformational Analysis of C8-Substituted Guanine Nucleotides in Solution. The conformational behavior of the C8-substituted guanine nucleotides in solution was investigated combining NMR data with molecular mechanics calculations (SI S8). Hence, the conformation of guanine nucleotides may be defined by three key structural features: the ribose puckering, the glycosidic torsion angle χ (H1′−C1′−N9−C8), and the exocyclic C4′−C5′ bond orientation.[27] Two basic geometries usually exist for the ribose puckering (C2′endo vs C3′endo), as well as for the glycosidic torsion angle (anti vs syn type).[28] The actual geometries in solution may be deduced by obtaining the vicinal H/H coupling constants for the furanose proton pairs, as well as by the key proton−proton NOEs data within the furanose ring and those at the natural or modified guanine base, and analyzing them in conjunction with molecular mechanics calculations. The experimental H/H vicinal coupling constants of each C8-substituted nucleotide were measured and compared (especially $J_{1'2'}$ and $J_{3',4'}$) to those expected by applying the generalized Karplus equation[29] to the geometries obtained by molecular mechanics calculations for the basic C2′-endo and C3′-endo ribose conformations (SI Figure S3-A). Thus, small values of $J_{1',2'}$ (<3 Hz) are characteristic of a predominant C3′-endo form, while medium-large values of $J_{1'2'}$ (ca. 7 Hz) correspond to major C2′-endo ribose conformations. Moreover, the expected $J_{1',2'}$ and $J_{3',4'}$ are strongly correlated, since for large $J_{1',2'}$ values, small $J_{3',4'}$ couplings are expected, as well as the opposite. From inspection of the J values gathered in SI Table S1, it can be deduced that most of the studied nucleotides present a major C2′-endo conformation (all $J_{1',2'}$ values were higher than 5.6 Hz). Nevertheless, the presence of a minor C3′-endo geometry can be also guessed, varying from ca. 15% to 30%. NOE data were also employed to assess the conformational equilibrium for the ribose ring. Obviously, for large $J_{1',2'}$ values, small NOE H1′-H2′ intensities are expected (major C2′-endo form), while for small $J_{1',2'}$ values, larger H1′-H2′ NOEs should take place (main C3′-endo conformer). In fact, weak H1′-H2′ NOE were found (Table S1). Concerning the glycosidic torsion angle χ, two basic conformational regions can be anticipated, depending on the orientation of the purine base relative to the ribose ring: the anti (χ ca. 180°), and the syn (χ ca. 80°) conformers (Figure 1-A). Previous conformational studies have proposed

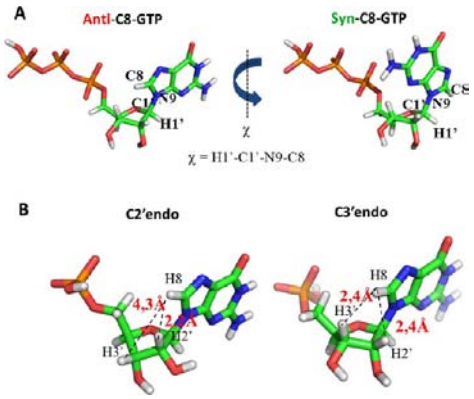

Figure 1. Guanosine nucleotide conformations. (A) glycosidic torsion angle: anti vs syn conformation. (B) ribose puckering, C2′endo vs C3′endo and characteristic distances.

that, for purine nucleotides with large substituents at C8, the syn conformation should be the major one existing in solution.[30] Alternatively, when the substituent at C8 is relatively small, a conformational equilibrium between the syn- and anti forms should take place.[31] Fittingly, the observed NOE pattern between the protons at the C8-substituent and the ribose protons has been proven to be useful to determine the conformation around the glycosidic linkage.[32]

Thus, the existence of strong NOE cross-peaks between ribose H1′ and the protons at the C8-substituent are indicative of the occurrence of a major syn conformation. In contrast, the presence of strong NOEs contacts between the ribose H2′ and/or H3′ with the protons at the C8-substituent strongly suggest that an antitype conformation is predominant. Since these NOE contacts are exclusive of each conformation, a careful analysis of the corresponding intensities should allow estimating, at least semiquantitatively, the relative abundance

Table 1. Binding Affinities of Guanine Nucleotide Analogs to FtsZ from Mj-FtsZ and Bs-FtsZ at 25°C

	Bs-FtsZ			Mj-FtsZ			
ligand	K_d (μM)	ΔG^0 (kcal mol^{-1})	$\Delta\Delta G^0$ GMP → GTP (kcal mol^{-1})	kd (μM)	ΔG^0 (kcal mol^{-1})	$\Delta\Delta G^0$ GMP → GTP (kcal mol^{-1})	$\Delta\Delta G^0$ Mj-FtsZ → Bs-FtsZ (kcal mol^{-1})
GTP	~0.033 ± 0.006	~−10.21 ± 0.10	~−4.20	~0.009 ± 0.005[a]	~−10.98 ± 0.25	~−4.96	~0.77
GMP	39.2 ± 5.0	−6.01 ± 0.07		38.2 ± 9.0	−6.02 ± 0.12		0.01
MorphGTP	0.274 ± 0.015[b]	−8.95 ± 0.04	−3.51	0.433 ± 0.008[a,c]	−8.67 ± 0.01	−3.72	−0.28
MorphGMP	103 ± 2	−5.44 ± 0.02		233 ± 42	−4.95 ± 0.10		−0.49
PyrrGTP	0.042 ± 0.001	−10.07 ± 0.02	−4.60	0.019 ± 0.006[a]	−10.52 ± 0.19	−5.50	0.45
PyrrGMP	97.1 ± 20.0	−5.47 ± 0.11		208 ± 30	−5.02 ± 0.06		−0.45
MeOGTP	0.010 ± 0.001	−10.90 ± 0.02	−4.68	0.006 ± 0.001[a]	~-11.2	−5.41	0.30
MeOGMP	27.6 ± 8.5	−6.22 ± 0.13		57.1 ± 24.6	−5.79 ± 0.19		−0.43
BrGTP	0.054 ± 0.015	−9.91 ± 0.14		0.079 ± 0.031[a]	−9.68 ± 0.58		−0.23

[a]Data from Schaffner-Barbero et al.[23] [b]0.173 ± 0.020 μM measured in Tris-D_2O buffer for NMR experiments [c]0.578 ± 0.140.μM measured in Tris-D_2O buffer for NMR experiments

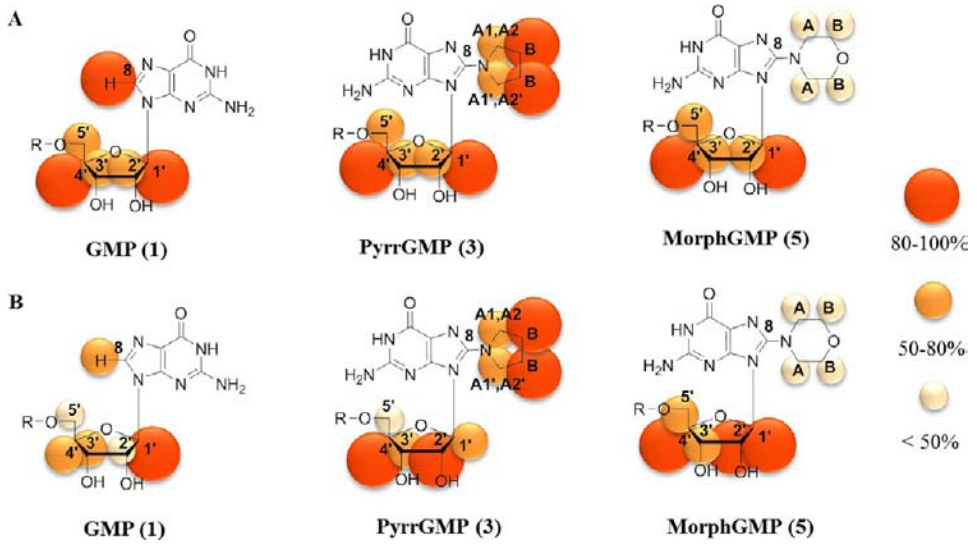

Figure 2. Epitope mapping of each C8-guanine nucleotides (**1**, **3**, and **5**) in the presence of FtsZ. (A) Mj-FtsZ (B) Bs-FtsZ.

of each conformer in solution (SI Table S2). Fittingly, although only for the particular case of anti type conformers, it is also expected that a correlation should exist between the relative intensities of the H8−H2′ and H8−H3′ NOEs with the predominant endo-C2′ and endo-C3′ geometries, respectively (Figure 1-B). The NOEs were interpreted using a full relaxation matrix approach with the Mspin program,[33] and employing the molecular mechanics-optimized anti- and syn-geometries for the calculations (SI S8). GMP (**1**) and GTP (**2**) adopt a major anti disposition in solution (ca. 80%) (SI Table S2). Moreover, the experimental H8−H2′ NOE is much larger than the H8−H3′ contact, indicating that the C2′-endo geometry is more populated than the C3′-endo alternative. Nevertheless, the existence of the H8−H3′ NOE indicated that the C3′-endo form is also present. In contrast, the pyrr (**3** and **4**) and morph (**5** and **6**) C8-modified nucleotides (mono and triphosphate), displayed the syn conformation as the exclusive form (SI Table S2), in agreement with the expectations.[34]

The conformation of the guanine nucleotides bound to FtsZ (Mj-FtsZ and Bs-FtsZ) was studied using a combination of saturation transfer difference (STD-NMR)[35] and transferred NOE (trNOESY)[36] experiments. The dissociation kinetics (high affinity) for the triphosphate nucleotides GTP (**2**), PyrrGTP (**4**), MorphGTP (**6**), was too slow to obtain satisfactory STD or trNOESY spectra. The observed high binding affinity of GDP (**23**) decided us to use the corresponding monophosphate analogs, which showed lower binding affinities and yielded good STD and trNOESY spectra. By substituting triphosphate nucleotides for monophosphate nucleotides, we are assuming that they bind to the same site in a similar way. This assumption was validated with fluorescence anisotropy (see below) and STD competition results (SI Figures S4 and S5), which confirmed that the GMP and GTP analogs bind in the same pocket. This indicated that the GMP analogs were proper models to study the interactions of FtsZ with C8-substituted guanine nucleotides.

Binding Affinities of C8 Nucleotide Analogs to Bs-FtsZ and Mj-FtsZ. Prior to the NMR experiments, we determined the binding affinities of the monophosphate nucleotides GMP (**1**), PyrrGMP (**3**), MorphGMP (**5**), and MeOGMP (**7**) and their triphosphate analogs. The inhibitory potency of these GTP analogs on eubacterial FtsZ from *E. coli* and *B. subtilis* had been shown to correlate with their affinity for the model archaeal Mj-FtsZ.[18,23] To determine the relationship between assembly inhibition and binding affinity for the same FtsZ species, we also performed affinity measurements on Bs-FtsZ, using the mant-GTP fluorescence anisotropy competition assay (see SI S3). The guanine nucleotide affinities for Bs-FtsZ and Mj-FtsZ are presented in Table 1. It can be observed that the binding affinities of these nucleotides to Mj-FtsZ and to Bs-

dx.doi.org/10.1021/ja405515r | J. Am. Chem. Soc. 2013, 135, 16418−16428

Table 2. Bioactive Glycosidic Conformation (Anti vs Syn) Of C8-Substituted Guanine Nucleotide Bound to Mj- and Bs-FtsZ Based on the Experimental NOE Intensities between the Protons at the C8-Substituent (X) and the Ribose Protons (H1′, H2′ and H3′)

nucleotide/FtsZ variant	NOEs involving C8-substituent (qualitative analysis) in the bound state[a]			bioactive anti-syn conformation	free state conformation (SI Tables S1 and S2)
	X–H1′	X–H2′	X–H3′		
GMP/*Mj-FtsZ*	n.d.[b]	strong	medium-strong	anti	80% C2′-endo 85% anti
GMP/*Bs-FtsZ*	n.d.[b]	strong	medium-strong	anti	
PyrrGMP/*Mj-FtsZ*	strong	n.d.[b]	n.d.[b]	syn	85% C2′-endo 100% syn
PyrrGMP/*Bs-FtsZ*	strong	n.d.[b]	n.d.[b]	syn	
MorphGMP/*Mj*-FtsZ	medium *X* = HA	medium *X* = HA weak *X* = HB	medium *X* = HB	anti/syn	85% C2′-endo 100% syn
MorphGMP/*Bs-FtsZ*	n.d.	strong *X* = HA medium *X* = HB	strong *X* = HB	anti	

[a]X = H8 for GMP and GTP; X = HA1/HA2 for pyrrGMP and pyrrGTP; and X = HA or HB for MorphGMP and MorphGTP. [b]n.d., not detected.

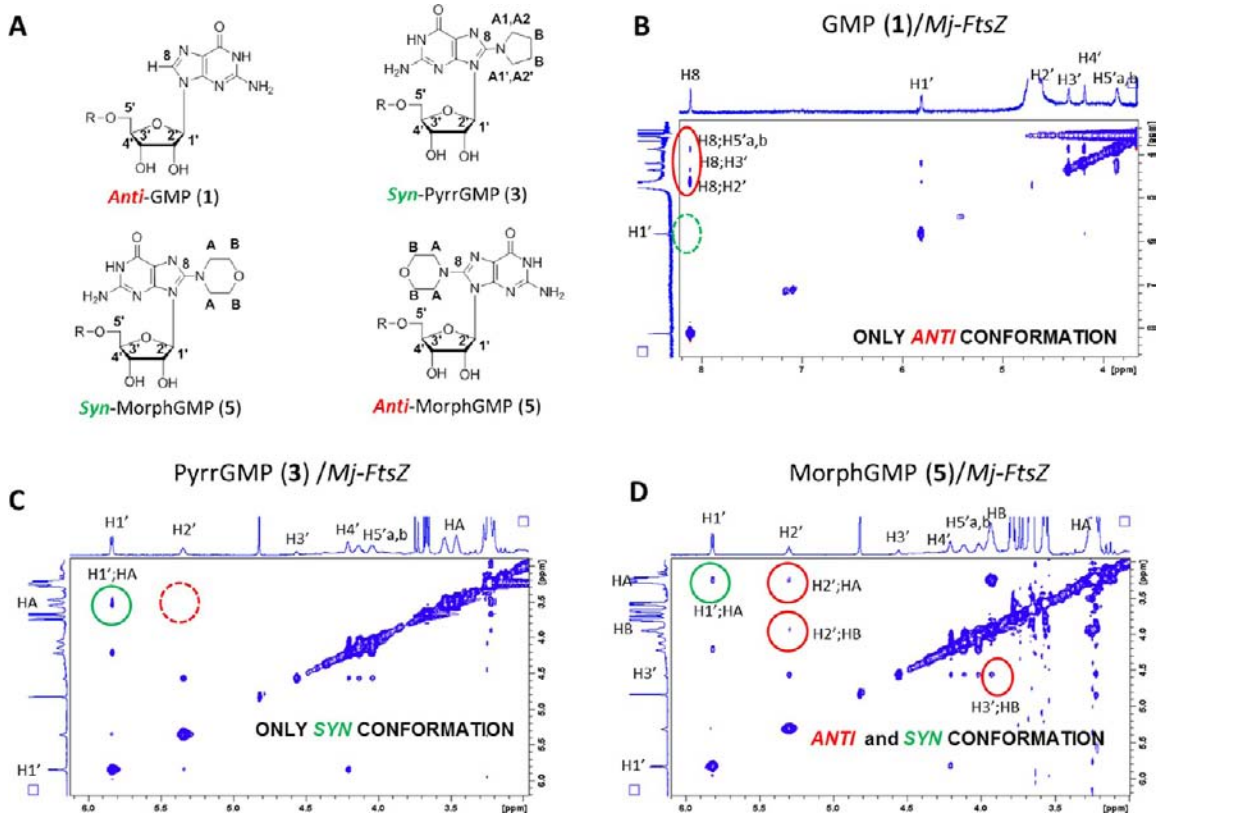

Figure 3. trNOESY of natural GMP and C8-substituted nucleotides in presence of Mj-FtsZ, ligand-protein ratio 20:1 at 298 K and 100 ms mixing time. (A) C8-substituted guanine nucleotides and numbering used in the NMR experiments. (B) trNOESY with GMP (**1**). (C) trNOESY with PyrrGMP (**3**). (D) trNOESY with MorphGMP (**5**).

FtsZ are very similar. In fact, the average difference in the binding free energy change of all ligands between both protein sites is only -0.21 ± 0.37 kcal mol^{-1}. These results indicate that the energetics of nucleotide binding to FtsZ is conserved,which is compatible with the high structural similarity of FtsZ binding sites from divergent organisms.[20] Comparing the binding free energy changes of the tri- and monophosphate guanine, Pyrr-, and MeO-nucleotides, the average apparent contribution to binding of the β- and γ-phosphates is $\Delta\Delta G^0$ (C8-GMP → C8-GTP) = ΔG^0C8-GTP − ΔG^0C8-GMP = -5.29 ± 0.17 kcal mol^{-1} for Mj-FtsZ and ΔG^0C8-GTP − ΔG^0C8-GMP = -4.50 ± 0.15 kcal mol^{-1} for Bs-FtsZ.

These results with the C8-analogs are fully compatible with previous ones with GTP, GDP, and GMP, which showed that the β-phosphate is important for binding; in fact, its removal decreases nucleotide affinity 1000-fold (ca. 4.1 kcal/mol). In contrast, the γ-phosphate contributes weakly to the observed nucleotide binding affinity.[23] In the case of the Morph-nucleotides, the apparent contribution of the β- and γ-phosphate groups is 1.0–1.5 kcal mol^{-1} lower than that for the other C8-substituted nucleotides (Table 1). This difference suggests that the morpholine group partially compromises the stabilizing contributions of the β- and γ-phosphates to binding.

Binding Epitope of the C8 Nucleotides to Mj-FtsZ and Bs-FtsZ Proteins as Deduced from STD Measurements. STD-NMR is a useful tool to detect ligand binding epitopes

dx.doi.org/10.1021/ja405515r | J. Am. Chem. Soc. 2013, 135, 16418–16428

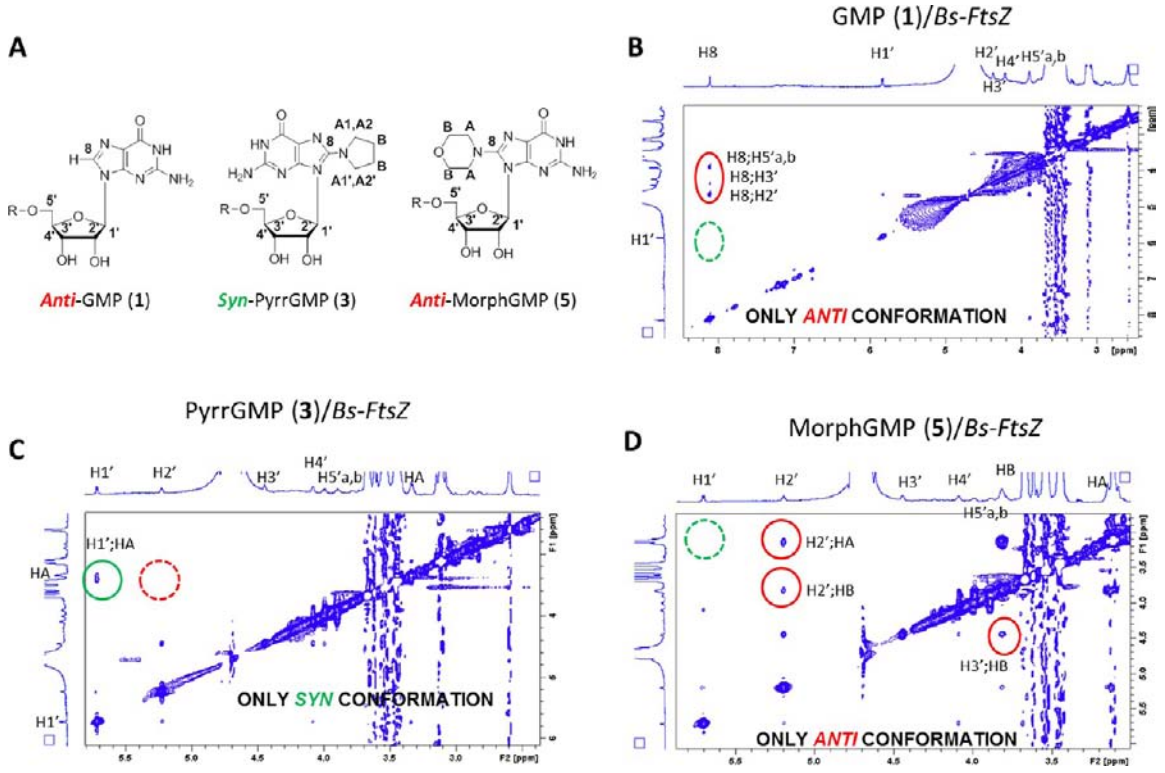

Figure 4. trNOESY of natural GMP and C8-substituted nucleotides in presence of Bs-FtsZ, ligand-protein ratio 20:1 at 298 K and 100 ms mixing time. (A) C8-substituted guanine nucleotides and numbering used on the NMR experiments. (B) trNOESY with GMP (**1**). (C) trNOESY with PyrrGMP (**3**). (D) trNOESY with MorphGMP (**5**).

interacting with receptors.[37] In fact, the analysis of the obtained data (Figures 2 and SI S6−S11) permits to point out the existence of significant differences in the binding mode of GMP and its C8-modified analogs to the two proteins. In particular, for GMP, H1′ of the ribose showed the highest percentage of saturation for both Mj-FtsZ and Bs-FtsZ. Small differences in the saturation of the guanine H8, ribose H2′, and both H5′ab protons could be appreciated, depending on the FtsZ species. In contrast, PyrrGMP showed a different binding epitope for both FtsZ proteins (Figures 2 and SI S12 and 13). Differences in the GMP epitope were appreciated, especially for Bs-FtsZ. It is noteworthy to mention the remarkable STD intensity observed for the HB protons at the pyrrolidine ring in this case. For MorphGMP, differences were also observed (Figures 2 and SI S12 and 13). It is important to address that the protons at the morpholine ring received much less saturation than their analogs in the pyrrolidine derivative.

^{31}P NMR experiments in absence and presence of Mj-FtsZ protein were also carried out, in order to understand the contribution of each phosphate moieties to the recognition process (SI Figure S14). These experiments also indicated that PyrrGTP and MorphGTP were not hydrolyzed by Mj-FtsZ (SI Figure S15).

Conformation of the C8-Substituted Nucleotides Bound to Mj-FtsZ and Bs-FtsZ Proteins—A trNOESY Analysis. Experiments were performed to assess the global geometry of the molecules in their bound states. The results presented below are summarized in Table 2.

Mj-FtsZ Case. For GMP bound to Mj-FtsZ, the observed H8−H2′ (strong) and H8−H3′ (medium-strong) NOEs cross-peaks (Figure 3-B) supported the unique presence of the anti conformation in the bound state, with a C3′-endo puckering of the furanose ring. The absence of the H8−H1′ NOE cross-peak indicated that only the anti conformation of GMP was selected (Figure 3-B). These observations are in agreement with the X-ray crystallographic structures (PDB 2vap and 1w5a) that show that both GDP and GTP adopt anti and C3′-endo conformations in their bound states.[5,20] For PyrrGMP exclusive NOEs indicating contacts between the pyrrolidine ring protons and ribose H1′ were detected, revealing that the syn conformer is bound in this case (Figure 3-C). No NOEs between the pyrrolidine protons and H2′ or H3′ were detected. For MorphGMP, the data indicated the existence of a mixture between the syn (NOE H1′−HA) and anti (NOEs H2′−HA, H2′−HB and H3′−HB) conformations (Figure 3-D). In principle, a qualitative analysis of the NOE intensities suggested a ca. 1:1 syn-anti distribution (Figure 3-D).

Bs-FtsZ Case. The trNOESY data of GMP natural ligand demonstrated the exclusive recognition of the anti conformation (NOEs H8−H2′; H8−H3′; H8−H5′a; and H8−H5′b) for Bs-FtsZ (Figure 4-B), in agreement with Bs-FtsZ-GDP and -GTPγS crystal complexes (PDB 2rhl and 2rho).

However, the data for PyrrGMP in the presence of Bs-FtsZ showed, as in the case of Mj-FtsZ, the exclusive recognition of the alternative syn conformation (Figure 4-C). Strikingly, the data for MorphGMP now indicated that only the anti geometry was selected by the Bs-FtsZ protein (Figure 4-D). These results point out the existence of different binding modes between the two FtsZ proteins for this molecule and that the interactions of Bs-FtsZ with PyrrGMP and MorphGMP are different (Table 2). Fittingly, Bs-FtsZ binding completely switches the glycosidic linkage conformation of MorphGMP from syn (free) to anti (when bound, Table 2). This conformational distortion is only partial for the Mj-FtsZ protein. This dramatic

dx.doi.org/10.1021/ja405515r | J. Am. Chem. Soc. 2013, 135, 16418−16428

conformational change may weaken the binding affinities of the MorphGMP/GTP analogs.

Further analysis of the trNOESY data revealed differences in the H1′−H4′ crosspeak intensities for PyrrGMP and MorphGMP. They are weak-medium for Bs-FtsZ and strong for Mj-FtsZ. This evidence was considered in the derivation of the 3D structure of the different complexes (see Discussion).

In summary, the analysis of the NMR data reveals the following: (i) conformational variation among the different analogs in the free state, (ii) the presence of drastic changes in the recognition of the analogs by FtsZ proteins from two different organisms, and (iii) a major conformational change between free and bound Morph-GMP (Table 2).

Different Inhibitory Effects of the C8-GTP Analogs on the Polymerization of Bacterial and Archaeal FtsZ. Following the analysis of the molecular recognition process of the C8-substituted GTP analogs by unassembled FtsZ, we proceeded to study the effects of the modified nucleotides on FtsZ polymerization. We observed that the assembly inhibitory potencies of the C8-substituted GTP analogs on FtsZ from *B. subtilis* (a Gram-positive bacterium) correlate with their binding affinities to this protein (Figure 5). A similar inhibition on the

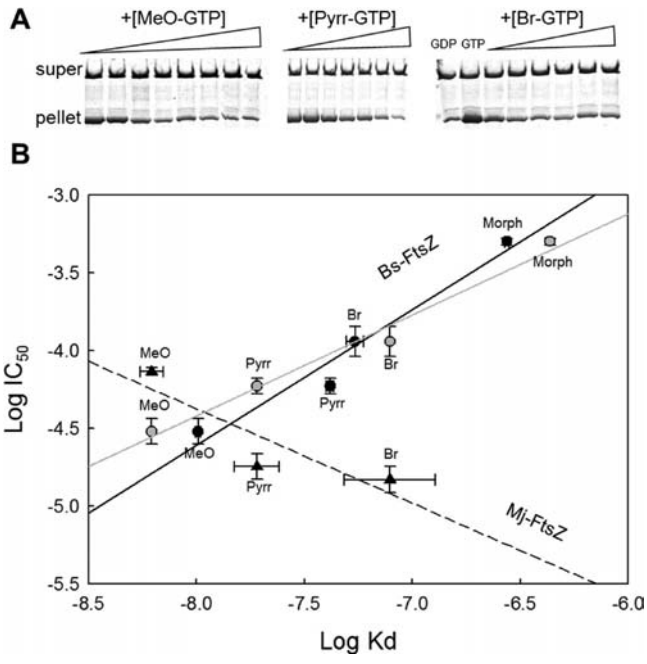

Figure 5. Inhibition of FtsZ assembly and binding affinity of the C8-substituted GTP analogs. (A) Inhibition of Mj-FtsZ polymerization by incrementing concentrations of MeOGTP, PyrrGTP, and Br-GTP. (B) Correlation of the polymerization inhibition (log IC50) with the dissociation constant using Mj-FtsZ (triangles; IC50 values determined in this study, K_d values from ref 23), compared to Bs-FtsZ (circles; K_d values determined in this study, IC50 values from ref 23). The previously determined interspecies correlation of logIC50 for Bs-FtsZ vs K_d for Mj-FtsZ[23] (gray circles) is shown here for comparison. The lines correspond to the best least-squares linear fits.

FtsZ from *E. coli* (a Gram-negative bacterium) has also been previously reported by us.[23] The inhibition of the assembly of Mj-FtsZ (from an archaea) by four nucleotide derivatives (MeOGTP, PyrrGTP, BrGTP, and MorphGTP) was measured employing a pelleting assay which determines the concentration of polymerized FtsZ. Unexpectedly, we found a different relationship of the assembly inhibitory capacity with the binding affinity of these compounds on Mj-FtsZ (Figure 5); the lower affinity analogs have a higher inhibition capacity on Mj-FtsZ. The IC50 values were as follows: MeOGTP 73.5 ± 4.3 μM; PyrrGTP 18.0 ± 3.8 μM; BrGTP 14.9 ± 3.1 μM. An important exception is MorphGTP, which was observed to enhance Mj-FtsZ polymerization. These results indicate that although archaeal Mj-FtsZ monomers contain a representative model nucleotide binding site, the Mj-FtsZ polymers are inhibited by the C8-analogs in a different fashion than that observed for Bs-FtsZ. This means that there must be differences at the association interface between the consecutive FtsZ monomers that provides the required interactions for completing the nucleotide binding site.[5,11b]

In a subsequent experiment, we observed that MorphGTP induces the nucleated polymerization of apo-Mj-FtsZ in the presence of Mg^{2+} and absence of any other nucleotide (Figure 6-A), with a critical concentration Cr = 1.00 ± 0.02 μM (Figure

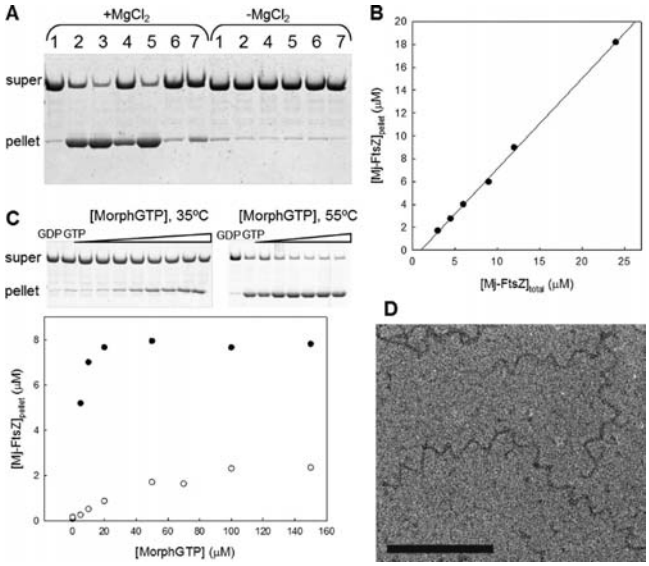

Figure 6. MorphGTP-induced polymerization of Mj-FtsZ. (A) Mj-FtsZ (9 μM) polymer pelleting assay in the presence of 1 mM GDP (**1**), 2 mM GTP (**2**), 0.5 mM GMPCPP (**3**), and the C8-derivatives of GTP at 0.1 mM: Br-GTP (**4**), Morph-GTP (**5**), Pyrr-GTP (**6**), and MeOGTP (**7**) in the presence and in the absence of 10 mM $MgCl_2$. (B) Mj-FtsZ polymerization with 0.1 mM MorphGTP. (C) Mj-FtsZ (9 μM) polymer pelleting in the presence of increasing concentrations of MorphGTP at two different temperatures: 35 °C (open circles) and 55 °C (filled circles) and quantification of polymer (bottom). (D) electron micrograph of Mj-FtsZ (9 μM) polymers with MorphGTP (0.1 mM) and $MgCl_2$ (10 mM) at 55 °C. Bar, 200 nm.

6-B). Titrations of Mj-FtsZ polymer formation with MorphGTP showed an increasing fraction of polymerized FtsZ, compatible with the binding of one MorphGTP molecule per FtsZ monomer at 55 °C (Figure 6-C). MorphGTP induced the assembly of Mj-FtsZ in wavy spiral-like polymers with one subunit thickness (5.5 ± 0.3 nm wide) (Figure 6-D). Fittingly, MorphGTP was not significantly hydrolyzed by Mj-FtsZ under these conditions (MorphGTPase activity = 0.0035 ± 0.0030 min^{-1}). No structured polymers, but only protein aggregates, were observed with the other three C8-derivatives of GTP and, as expected, no GTPase activity was detected. The FtsZ polymers with MorphGTP are morphologically similar to those formed by Mj-FtsZ with GDP and crowding agents,[22] and closely similar to those formed by the Mj-FtsZ C-terminal

dx.doi.org/10.1021/ja405515r | J. Am. Chem. Soc. 2013, 135, 16418−16428

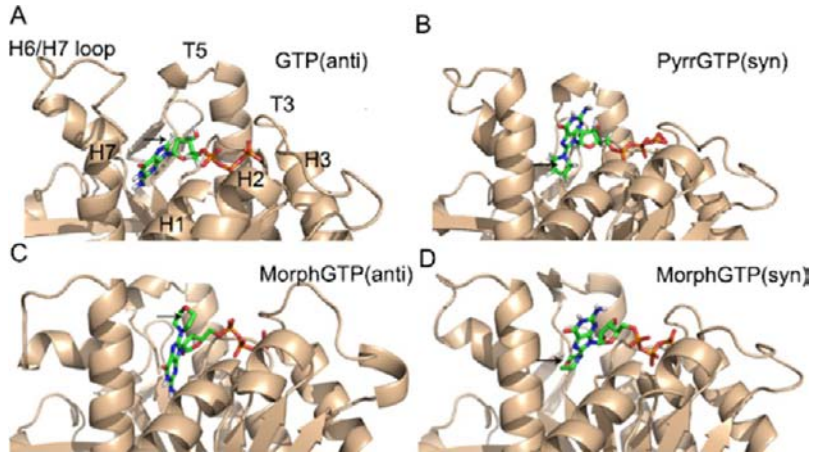

Figure 7. Binding poses of modified analogs in the Mj-FtsZ nucleotide site. GMP and C8-substituted monophosphate analogs in the NMR-determined bound conformation were docked and extended to the corresponding triphosphate. Stable structures averaged over the last 0.5 ns of MD simulation are represented. The arrows point to the C8-substituents.

domain mutants G320V and H288A. We have reported that these mutants prevent the curved-to-straight transition of FtsZ upon assembly, locking the FtsZ filaments in a curved conformation and inhibiting the GTPase activity.[16b] Thus, these observations suggest that the binding of MorphGTP instead of GTP inhibits the conformational change of Mj-FtsZ to an active-straight conformation and affects the contact with the monomer above. In summary, the inhibitory potencies of MeOGTP, PyrrGTP, BrGTP, and MorphGTP on the assembly of Bs-FtsZ correlate with their binding affinities. However, this is not the case for Mj-FtsZ. For this species, MorphGTP behaves as a nonhydrolyzable nucleotide analog whose binding induces the formation of curved filaments of Mj-FtsZ that resemble the polymerization products of the inactive forms of this protein.

■ DISCUSSION

Different Poses of C8 Nucleotides on the Binding Site of FtsZ—Matching the NMR Data with Molecular Models. The NMR results contain key structural information defining the bioactive conformations of the natural and modified nucleotide analogs. The changes of conformations between free and bound analogs and between the two FtsZ species indicate the existence of a delicate balance of enthalpy and entropy factors in the recognition of these molecules. Although it is tempting to try to derive a structure−function relationship based on these conformational changes, care should be taken for the extrapolation of these structural data to the distinct functional behavior observed for these molecules with the two proteins. Thus, molecular modeling protocols were applied to get insights into the structural details of the molecular recognition process and the inhibition of FtsZ assembly. The GMP derivatives were first docked onto Mj-FtsZ and Bs-FtsZ monomers, respectively employing the PDB 1w5a and 2vxy crystal structures, using the protocol described in the SI (page S7, Figures S16, S17). Only the poses with glycosidic conformation in agreement with the NMR data and 3′-endo ribose puckering were selected from the good-scoring docking solutions obtained with Autodock 4.2.[38] The different docking poses of PyrrGMP and MorphGMP and their interactions with Mj-FtsZ and Bs-FtsZ binding sites were analyzed (SI Figures S18−21). Since the docking protocol only provides a static perspective of the interaction, the nucleotide monophosphates were then extended to the corresponding triphosphates and their complexes with Mj-FtsZ were subjected to MD simulations (SI Figures S22−23). The resulting model complexes showed different binding poses of the C8-substituted nucleotides and structural rearrangements around the binding site (Figure 7). GTP binds in an anti conformation, thus maintaining its major conformation in the free state. However, the ribose puckering changes from a predominantly 2′-endo in the free state to 3′-endo in all of the analyzed FtsZ-bound guanine nucleotides. The GTP-FtsZ model complex (Figure 7-A) is very similar to the initial crystallographic structure 1w5a (SI Figure S22), thus validating the MD protocol. PyrrGTP adopts a bound syn conformation in the model complex, maintaining the solution conformation around the glycosidic linkage.

However, there is a large rearrangement with respect to bound GTP. The pyrrolidine ring replaces the six-member ring of the guanine nucleobase, which has flipped into a new orientation toward the outside of the binding site (Figure 7-B). The pyrrolidine ring makes stabilizing contacts with helices H6 and H1, and the γ phosphate lacks hydrogen bonding with loop T3. MorphGTP, which has a syn conformation in solution, binds both in the anti and syn conformers to Mj-FtsZ (Figure 7-C,D). The anti conformer provides better intermolecular interactions with the protein and is probably favored by enthalpy reasons. However, the recognition of the syn-conformer does not require an entropy penalization. Therefore, the free energy difference between both states is minimized and the protein recognizes both forms. The anti conformer binds in a pose similar to that of GTP, which is also similar to that described for MorphGTP in the complex with FtsZ from *Aquifex aeolicus* (PDB 2r75).[18] The morpholine ring is oriented outward from the binding site weakening the interactions of the γ-phosphate with loop T3 relative to GTP. The syn-conformer of MorphGTP is recognized in a binding pose similar to that of PyrrGTP, with the C8-substituent into the binding site and the guanine nucleobase pointing outward, yet maintaining its hydrogen bonds to loop T3. Like Mj-FtsZ, Bs-FtsZ recognizes PyrrGMP in the same syn conformation of the free nucleotide. However, in contrast with Mj-FtsZ, Bs-FtsZ only recognized the anti conformer of MorphGMP, which is not found in the free ligand. This may be attributed to the binding pocket of Bs-FtsZ being narrower than Mj-FtsZ's (SI Figures S24−25) and

dx.doi.org/10.1021/ja405515r | J. Am. Chem. Soc. 2013, 135, 16418−16428

the morpholine ring being larger than the pyrrolidine ring. In fact, docking calculations did not provide any solutions with the morpholine ring embedded within the Bs-FtsZ binding site (in the syn conformation). Furthermore, the derived 3D geometries permitted to rationalize the observed differences in the H1′−H4′ NOEs for the Bs-FtsZ versus the Mj-FtsZ complexes (see spin diffusion effects in SI, page S27).

Effect of C8-Substituted GTP Analogs at the FtsZ Association Interface and Their Inhibition Mechanisms. The nucleotide binding site is at the plus end of the FtsZ molecule, making contacts with the next monomer along the FtsZ filament, as shown by the structure of a filament-like Mj-FtsZ dimer (PDB 1w5a).[5] The nucleotide site is fairly accessible in this structure (Figure 8-A). A model Bs-FtsZ dimer was initially constructed by aligning the monomer Bs-FtsZ structure (PDB 2vxy) onto the Mj-FtsZ dimer, resulting in a similarly accessible nucleotide binding site. However, a new filament interphase has recently become available with the structures of Sa-FtsZ (PDB 3vo8, 4dxd).[11a,b] Therein, the C-terminal domain is reoriented in an open conformation with respect to the N-terminal domain, while the core H7 helix and loop T7 slid down, providing a possible structural mechanism for the FtsZ assembly switch.[16b] This rearrangement generates much closer contacts between the two Sa-FtsZ monomers, thus burying the nucleotide. Fittingly, Bs-FtsZ displays a 80% sequence identity with the ordered residues in the Sa-FtsZ crystal structures, and a 100% identity in the nucleotide binding pocket.[11a] Thus, a similar Bs-FtsZ dimer model structure was created by homology to the Sa-FtsZ filament (Figure 8-B).

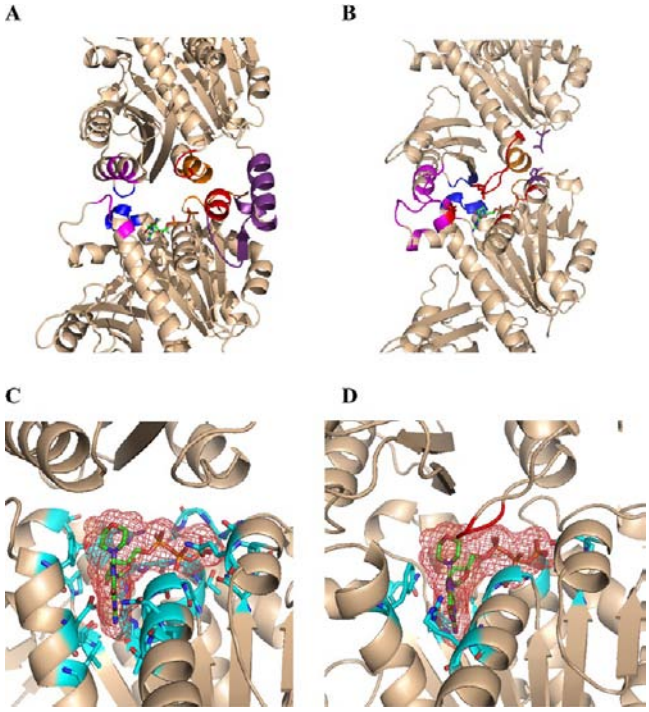

Figure 8. (A) Mj-FtsZ dimer structure with bound GTP (PDB 1w5a). The protein−protein contacts are colored. (B) Bs-FtsZ (PDB 2vxy) dimer modeled by homology onto the Sa-FtsZ filament structure (PDB 3vo8, with GDP extended to GTP; see SI page S28). The contacts are colored. (C) Mj-FtsZ dimer (PDB 1w5a) with MorphGTP in the anticonformer. MorphGTP is enclosed by its envelope (red mesh) and the contacting protein side chains are highlighted (magenta sticks). (D) Superposition of MorphGTP (anticonformer) onto the Bs-FtsZ dimer model. Steric clashes of the main chain of loop T7 (Ile207, Ans208) from the upper monomer with the morpholine group are indicated in red. Similar steric clashes were found introducing MorphGTP into the Sa-FtsZ structure (PDB 1vo8). Similar conclusions were obtained by employing Z-Docking (see SI S28).

In the case of Mj-FtsZ, the C8-substituent of the anticonformers and the swapped guanine of the syn-conformers of the GTP analogs point toward the contacting monomer in all cases. From a merely steric perspective, the active site cavity of the archaeal Mj-FtsZ dimer could accommodate the C8-substituents (Figure 8-C). Indeed, the Mj-FtsZ monomers do not get closer, and the cavity retains its initial volume throughout extensive MD simulations.[39] However, it is evident that the C8-substituents introduce changes in size, shape, and electrostatic surface at the interface. The observed inhibition of assembly does not directly relate to the analogs binding in either anti- or syn conformations, but very probably to remodeling of the monomer−monomer interface caused by the presence of the C8-substituent. We suggest that this remodeling originates from (i) the large electrostatic changes due to the introduction of the morpholine or guanine groups exposed at the dimer interface, as well as by (ii) small displacements of the contact elements, particularly at the N-terminal end of helix H7 and loop T3, which are induced by their different interactions with the C8-substituted analogs (SI Figure S23). This type of hypothesis may explain the MorphGTP-induced polymerization of Mj-FtsZ into curved filaments, which are characteristic of inactive FtsZ (Figure 6-D), since these perturbations are expected to result in additional monomer−monomer interactions. The initial Bs-FtsZ dimer model built onto the Mj-FtsZ dimer lead to similar explanations for the effects of the C8-nucleotide analogs as for Mj-FtsZ.

However, a simpler explanation for the inhibition of bacterial FtsZ polymerization by the C8-substituted GTP analogs is provided by the new Sa-FtsZ structure[11a,b] and by the Bs-FtsZ homology model presented here. In this case, the C8-modified nucleotides cannot fit into the close interface (Figure 8-D), related to the lower position of H7-T7 from the upper subunit. In fact, the observed correlation between the inhibition of polymerization and their affinity of binding to the nucleotide site (Figure 8) suggests a direct competition of the binding of the C8-nucleotide analogs with the protein−protein interactions at the association interface between bacterial FtsZ monomers. This is also online with previous indications[11a] that small molecules as those presented herein and others discussed above (as PC190723) modulate the assembly of FtsZ protein by inducing conformational changes at the protein−protein interface.

■ CONCLUSIONS

NMR spectroscopy experiments have permitted the unraveling of the fine structural details of the molecular recognition of C8-substituted nucleotide inhibitors by the bacterial cell-division protein FtsZ. The combination of these results with biochemical measurements and molecular modeling approaches indicates that the C8-adducts generate significant changes in size, shape, and electrostatic surface at the interface between FtsZ monomers, which probably lead to the observed inhibition of the FtsZ assembly.

■ ASSOCIATED CONTENT

Supporting Information

Additional experimental details concerning the NMR conformational and binding studies, biochemical techniques, and computational methods. This material is available free of charge via the Internet at http://pubs.acs.org.

■ AUTHOR INFORMATION

Corresponding Author

jjbarbero@cib.csic.es; j.m.andreu@cib.csic.es

Present Address

[▽]Repsol, Technology Center, Móstoles, E-28923 Madrid, Spain

Author Contributions

[#]These authors contributed equally to the work.

Notes

The authors declare no competing financial interest.

■ ACKNOWLEDGMENTS

We thank Dr. T. Läppchen and Dr. T. den Blaauwen (Univ. of Amsterdam) for gifts of MeOGTP and PyrrGTP and for the studies which have instigated this one. We acknowledge financial support by grants from Spanish MINECO CTQ2011-22724 (S.M.S.), CTQ2012-32025 (J.J.B.) and BFU2011-23416 (J.M.A.), from Comunidad de Madrid CM S2010/BMD-2353 (J.J.B., J.M.A.), CM S2010-BMD-2457 (A.M.), from Fundación Severo Ochoa through the AMAROUTO program (A.M.) and the European Comission granted BM1003 and CM1102 COST actions. We thank CESGA Supercomputing Center for computational resources and UCM CAI-NMR. F.M. thanks FCT-Portugal for a postdoc grant (SFRH/BPD/65462/2009). We also thank Dr. Douglas V. Laurents for careful reading of the manuscript.

■ REFERENCES

(1) (a) Vollmer, W. *Appl. Microbiol. Biotechnol.* **2006**, *73*, 37−47. (b) Lock, R. L.; Harry, E. J. *Nat. Rev. Drug Discov.* **2008**, *7*, 324−338.

(2) (a) Payne, D. J. *Science* **2008**, *321*, 1644−1645. (b) Fischbach, M. A.; Walsh, C. T. *Science* **2009**, *325*, 1089−1093.

(3) (a) Adams, D. W.; Errington, J. *Nat. Rev. Microbiol.* **2009**, *7*, 642−653. (b) Egan, A. J. F.; Vollmer, W. *Ann. N.Y. Acad. Sci.* **2013**, *1277*, 8−28.

(4) (a) Nogales, E.; Downing, K. H.; Amos, L. A.; Lowe, J. *Nat. Struct. Biol.* **1998**, *5*, 451−458.

(5) Oliva, M. A.; Cordell, S. C.; Lowe, J. *Nat. Struct. Mol. Biol.* **2004**, *11*, 1243−1250.

(6) Erickson, H. P.; Anderson, D. E.; Osawa, M. *Microbiol. Mol. Biol. Rev.* **2010**, *74*, 504−528.

(7) Li, Z.; Trimble, M. J.; Brun, Y. V.; Jensen, G. J. *EMBO J.* **2007**, *26*, 4694−4708.

(8) Strauss, M. P.; Liew, A. T. F.; Turnbull, L.; Whitchurch, C. B.; Monahan, L. G.; Harry, E. J. *PLoS Biol.* **2012**, *10*, e1001389.

(9) (a) Vollmer, W. *Chem. Biol.* **2008**, *15*, 93−94. (b) Foss, M. H.; Eun, Y. J.; Weibel, D. B. *Biochemistry* **2011**, *50*, 7719−7734. (c) Schaffner-Barbero, C.; Martin-Fontecha, M.; Chacon, P.; Andreu, J. M. *ACS Chem. Biol.* **2012**, *7*, 268−276.

(10) Haydon, D. J.; Stokes, N. R.; Ure, R.; Galbraith, G.; Bennett, J. M.; Brown, D. R.; Baker, P. J.; Barynin, V. V.; Rice, D. W.; Sedelnikova, S. E.; Heal, J. R.; Sheridan, J. M.; Aiwale, S. T.; Chauhan, P. K.; Srivastava, A.; Taneja, A.; Collins, I.; Errington, J.; Czaplewski, L. G. *Science* **2008**, *321*, 1673−1675.

(11) (a) Elsen, N. L.; Lu, J.; Parthasarathy, G.; Reid, J. C.; Sharma, S.; Soisson, S. M.; Lumb, K. J. *J. Am. Chem. Soc.* **2012**, *134*, 12342−12345. (b) Matsui, T.; Yamane, J.; Mogi, N.; Yamaguchi, H.; Takemoto, H.; Yao, M.; Tanaka, I. *Acta Crystallogr., D: Biol. Crystallogr.* **2012**, *68*, 1175−1188.

(12) Andreu, J. M.; Schaffner-Barbero, C.; Huecas, S.; Alonso, D.; Lopez-Rodriguez, M. L.; Ruiz-Avila, L. B.; Nunez-Ramirez, R.; Llorca, O.; Martin-Galiano, A. J. *J. Biol. Chem.* **2010**, *285*, 14239−14246.

(13) Adams, D. W.; Wu, L. J.; Czaplewski, L. G.; Errington, J. *Mol. Microbiol.* **2011**, *80*, 68−84.

(14) Plaza, A.; Keffer, J. L.; Bifulco, G.; Lloyd, J. R.; Bewley, C. A. *J. Am. Chem. Soc.* **2010**, *132*, 9069−9077.

(15) Cherfils, J.; Zeghouf, M. *Nat. Chem. Biol.* **2011**, *7*, 493−495.

(16) (a) Huecas, S.; Llorca, O.; Boskovic, J.; Martin-Benito, J.; Valpuesta, J. M.; Andreu, J. M. *Biophys. J.* **2008**, *94*, 1796−1806. (b) Martin-Galiano, A. J.; Buey, R. M.; Cabezas, M.; Andreu, J. M. *J. Biol. Chem.* **2010**, *285*, 22554−22565.

(17) Läppchen, T.; Hartog, A. F.; Pinas, V. A.; Koomen, G. J.; den Blaauwen, T. *Biochemistry* **2005**, *44*, 7879−7884.

(18) Läppchen, T.; Pinas, V. A.; Hartog, A. F.; Koomen, G. J.; Schaffner-Barbero, C.; Andreu, J. M.; Trambaiolo, D.; Lowe, J.; Juhem, A.; Popov, A. V.; den Blaauwen, T. *Chem. Biol.* **2008**, *15*, 189−199.

(19) Hritz, J.; Läppchen, T.; Oostenbrink, C. *Eur. Biophys. J.* **2010**, *39*, 1573−1580.

(20) Oliva, M. A.; Trambaiolo, D.; Lowe, J. *J. Mol. Biol.* **2007**, *373*, 1229−1242.

(21) Huecas, S.; Andreu, J. M. *J. Biol. Chem.* **2003**, *278*, 46146−46154.

(22) Huecas, S.; Andreu, J. M. *FEBS Lett.* **2004**, *569*, 43−48.

(23) Schaffner-Barbero, C.; Gil-Redondo, R.; Ruiz-Avila, L. B.; Huecas, S.; Läppchen, T.; den Blaauwen, T.; Diaz, J. F.; Morreale, A.; Andreu, J. M. *Biochemistry* **2010**, *49*, 10458−10472.

(24) Schuck, P.; Perugini, M. A.; Gonzales, N. R.; Howlett, G. J.; Schubert, D. *Biophys. J.* **2002**, *82*, 1096−1111.

(25) Rivas, G.; López, A.; Mingorance, J.; Ferrándiz, M. J.; Zorrilla, S.; Minton, A. P.; Vicente, M.; Andreu, J. M. *J. Biol. Chem.* **2000**, *275*, 11740−11749.

(26) Case, D. A.; Darden, T. A.; Cheatham III, T. E.; Simmerling, C. L.; Wang, J.; Duke, R. E.; Luo, R.; Walker, R. C.; Zhang, W.; Merz, K. M.; Roberts, B.; Wang, B.; Hayik, S.; Roitberg, A.; Seabra, G.; Kolossváry, I.; Wong, K. F.; Paesani, F.; Vanicek, J.; Liu, J.; Wu, X.; Brozell, S. R.; Steinbrecher, T.; Gohlke, H.; Cai, Q.; Ye, X.; Wang, J.; Hsieh, M.-J.; Cui, G.; Roe, D. R.; Mathews, D. H.; Seetin, M. G.; Sagui, C.; Babin, V.; Luchko, T.; Gusarov, S.; Kovalenko, A.; Kollman, P. A. *AMBER 11*; Univ. of California: San Francisco, 2010.

(27) Sarma, R. H.; Lee, C.-H.; Evans, F. E.; Yathindra, N.; Sundaralingam, M. *J. Am. Chem. Soc.* **1974**, *96*, 7337−7348.

(28) Davies, D. B. *Prog. NMR Spectrosc.* **1978**, *12*, 135−225.

(29) Haasnoot, C. A. G.; de Leeuw, F. A. A. M.; Altona, C. *Tetrahedron* **1980**, *36*, 2783−2792.

(30) (a) Tavale, S. S.; Sobell, H. M. *J. Mol. Biol.* **1970**, *48*, 109−123. (b) Birnbaum, G. I.; Shugar, D. *Biochim. Biophys. Acta* **1978**, *517*, 500−510.

(31) Son, T.-D.; Guschlbauer, W.; Guéron, M. *J. Am. Chem. Soc.* **1972**, *94*, 7903−7911.

(32) Rosemeyer, H.; Tóth, G.; Golankiewicz, G.; Kazimierczuk, Z.; Bourgeois, W.; Kretschmer, U.; Muth, H.-P.; Seela, F. *J. Org. Chem.* **1990**, *55*, 5784−5790.

(33) *MSpin, version 1.2*; MestReLab Res. S.L.: S. Compostela, Spain, 2008.

(34) Evans, F. E.; Kaplan, N. O. *J. Biol. Chem.* **1976**, *251*, 6791−6797.

(35) (a) Mayer, M.; Meyer, B. *Angew. Chem., Int. Ed.* **1999**, *38*, 1784−1788. (b) Mayer, M.; Meyer, B. *J. Am. Chem. Soc.* **2001**, *123*, 6108−6117. (c) Meyer, B.; Peters, T. *Angew. Chem., Int. Ed.* **2003**, *42*, 864−890.

(36) Jiménez-Barbero, J., Peters, T. In *NMR Spectroscopy of Glycoconjugates*; Jiménez-Barbero, J., Peters, T., Eds.; Wiley: Weinheim, 2002, pp 289−310.

(37) (a) Canales, A.; Rodríguez-Salarichs, J.; Trigili, C.; Nieto, L.; Coderch, C.; Andreu, J. M.; Paterson, I.; Jiménez-Barbero, J.; Díaz, J. F. *ACS Chem. Biol.* **2011**, *6*, 789−799. (b) Jiménez-Barbero, J.;

Canales, A.; Northcote, P. T.; Buey, R. M.; Andreu, J. M.; Díaz, J. F. *J. Am. Chem. Soc.* **2006**, *128*, 8757−8765.
(38) Morris, G. M.; Huey, R.; Lindstrom, W.; Sanner, M. F.; Belew, R. K.; Goodsell, D. S.; Olson, A. J. *J. Comput. Chem.* **2009**, *16*, 2785−2791.
(39) (a) Hsin, J.; Gopinathan, A.; Huang, K. C. *Proc. Nat. Am. Soc.* **2012**, *109*, 9432−9437.